



ELSEVIER

Contents lists available at ScienceDirect

## Pattern Recognition

journal homepage: [www.elsevier.com/locate/pr](http://www.elsevier.com/locate/pr)

## Visual enhancement of old documents with hyperspectral imaging

Seon Joo Kim\*, Fanbo Deng, Michael S. Brown

National University of Singapore, Singapore

## ARTICLE INFO

## Article history:

Received 19 May 2010

Received in revised form

16 September 2010

Accepted 25 December 2010

## Keywords:

Hyperspectral imaging

Image fusion

Document processing and analysis

## ABSTRACT

Hyperspectral imaging (HSI) of historical documents is becoming more common at national libraries and archives. HSI is useful for many tasks related to document conservation and management as it provides detailed quantitative measurements of the spectral reflectance of the document that is not limited to the visible spectrum. In this paper, we focus on how to use the invisible spectra, most notably near-infrared (NIR) bands, to assist in visually enhancing old documents. Specifically, we demonstrate how to use the invisible bands to improve the visual quality of text-based documents corrupted with undesired artifacts such as ink-bleed, ink-corrosion, and foxing. For documents of line drawings that suffer from low contrast, we use details found in the invisible bands to enhance legibility. The key components of our framework involve detecting regions in the document that can be enhanced by the NIR spectra, compositing the enhanced gradient map using the NIR bands, and reconstructing the final image from the composited gradients. This work is part of a collaborative effort with the Nationaal Archief of the Netherlands (NAN) and Art Innovation, a manufacturer of hyperspectral imaging hardware designed specially for historical documents. Our approach is evaluated on historical documents from NAN that exhibit degradations common to documents found in most archives and libraries.

© 2011 Elsevier Ltd. All rights reserved.

## 1. Introduction

Hyperspectral imaging (HSI) captures a densely sampled spectral response of a scene object over a broad spectrum including invisible spectra such as ultra-violet (UV) and near-infrared (NIR). Hyperspectral imaging has been employed in various scientific disciplines to provide valuable data for fields such as astronomy [1,2], earth science and remote sensing [3,4], and computer vision [5]. With the advances in technology and cost reductions, hyperspectral imaging of historical art works and documents is now accessible for use in national libraries and archives [6,7].

One advantage of HSI in document imaging over the standard 3-channel imaging (i.e. RGB) is that HSI provides a detailed quantitative measurements of the document spectral response. Traditional RGB imaging, on the other hand, contains only a subset of the information available by combining response of all visible electro-magnetic (EM) radiation into three bands. This makes HSI more suitable for tasks that require accurate quantitative measurement such as conservation, detecting damage, and analysis of features in the document (e.g. ink and pigments) and changes over time due to aging or light exposure. In addition,

hyperspectral imaging provides measurements in the invisible spectrums (NIR, UV) which further enrich the analysis and enhancement of the data. Measurements in the invisible spectral bands provide more information about the document being imaged by sometimes seeing more than the visible range and by sometimes seeing less. This is demonstrated by two examples in Fig. 1. For the first example, the NIR band at 900 nm (Fig. 1(b)) provides more salient gradient details than the document in the visible band at 500 nm (Fig. 1(a)). Conversely, for the second example, the NIR band at 800 nm (Fig. 1(d)) is better for guiding enhancement than the 450 nm visible band (Fig. 1(c)) since artifacts such as ink-bleed and ink-corrosion are less prevalent.

The goal of this paper is to take advantage of hyperspectral images of historical documents to visually enhance the document's content by exploiting additional information provided by the NIR bands. The visual enhancement in this paper is applied to the RGB image of the hyperspectral data as the RGB image is the most natural visualization of the data. In this work, we are interested in two tasks. For the text-based documents that are corrupted with artifacts such as ink-bleed, corrosion, and foxing, we use the invisible bands which capture much less artifacts than the visible bands to clean up the artifacts in the documents while preserving the look and the feel of the original document. For drawing-based documents that contain low contrast regions, we use NIR bands which capture more details than the visible bands

\* Corresponding author.

E-mail address: [seonjookim@gmail.com](mailto:seonjookim@gmail.com) (S.J. Kim).

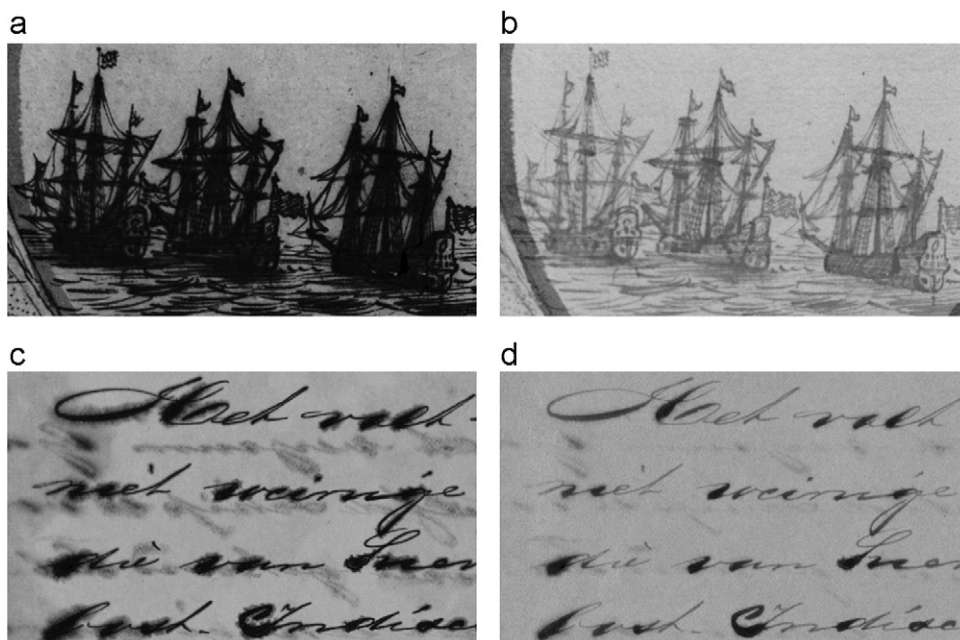


**Fig. 1.** Hyperspectral imaging provides measurements in invisible spectral ranges which helps to improve data analysis. In the first example, the image in the NIR band (b) captures more details of the image content which is barely seen in the visible band (a). In the second example, the NIR image (d) is useful because it does not exhibit as many undesired artifacts as the visible bands (c). (a) 500 nm. (b) 900 nm. (c) 450 nm. (d) 800 nm.

to enhance the contrast in the documents. The data are enhanced in the gradient domain which has been shown to be effective for many computer vision tasks such as image editing [8], contrast adjustment [9], image stitching [10], and intrinsic image computation [11]. The key components of our algorithm include detecting regions that can be enhanced by the additional NIR spectral images, compositing the enhanced gradient map from NIR images, and reconstructing the final image from gradients using an optimization scheme.

This work is a part of ongoing collaborative effort with the Nationaal Archief of the Netherlands (NAN), one of Europe's leading research archives, and Art Innovation, a manufacturer of hyperspectral imaging hardware designed for historical documents. The documents processed in this paper, which are indicative to the type of artifacts common to historical documents, are imaged at the NAN using the SEPIA Quantitative Hyper-Spectral Imager (QHSI) device developed by Art Innovation [12]. The device performs hyperspectral imaging by capturing a very narrow spectral band of EM radiation one at a time by placing a bandpass filter in front of the light source to block out all but a selected band of the EM spectrum. A monochromatic camera is then used to capture the amount of light that is reflected by the document at that selected band. The filter is changed for each image, thus capturing different parts of EM spectrum to build up the HSI (Fig. 2).

The QSHI device captures images at different wavelength bands from 365 (UV) to 1100 nm (near-infrared (NIR)) with the step size of 10 nm in most cases except the bands in 300 and 1000 nm's. The images have the resolution of 4 mega pixels ( $2048 \times 2048$ ) for a physical surface area of 125 mm  $\times$  125 mm and are captured at 16 bit per pixel. Such high-resolution (approximately 256 pixels per mm<sup>2</sup>) provides a reliable spatial measurement suitable for even thin lines of handwriting and printed text.

The remainder of the paper is organized as follows: we begin by reviewing related work in Section 2. In Section 3, we introduce our algorithm for visually enhancing old documents using the hyperspectral data. We show experimental results in

Section 4 and conclude with a discussion about our algorithm and future work.

## 2. Related work

As hyperspectral imaging is a relatively new procedure in libraries and archives, less existing work is available in the context of document processing. Here related works are discussed in the areas of document processing and image fusion, with more emphasis placed on image fusion given the larger body of relevant work.

### 2.1. Document processing

The majority of existing work for historical document processing focus on standard 3-channel (RGB) imaging (e.g. representative examples include [13–16]). In this area, the closest related works have focused on ink-bleed correction. However, these approaches have no additional benefits of spectral bands and thus have to make prior assumptions about the ink-corrosion [14,17,18] or enlist the help of the user in the form of training-data [15,19]. In addition, these approaches only consider classification of the ink-bleed, the final output is a binary image—there is no mechanism to preserve the look and feel of the original document.

Applying multispectral imaging to historical document is addressed in the work on Archimedes Palimpsest [20,21]. The Archimedes Palimpsest is a manuscript containing several treatises by Archimedes that was erased, overwritten and bound into a prayer book 800 years ago [20]. Works on this data concentrate on separating different sources of writing to recover the erased Archimedes writings. The data are assumed to be a linear mixture of different patterns (writings) and different methods for the source separation such as spectral unmixing [20] and independent component analysis (ICA) are used to recover the hidden texts. Although the work in [20,21] share a similarity with the use of spectral imaging, the goal set forth in our work differ. In particular, we are interested in enhancing the document while maintaining the look-and-feel of the original documents as

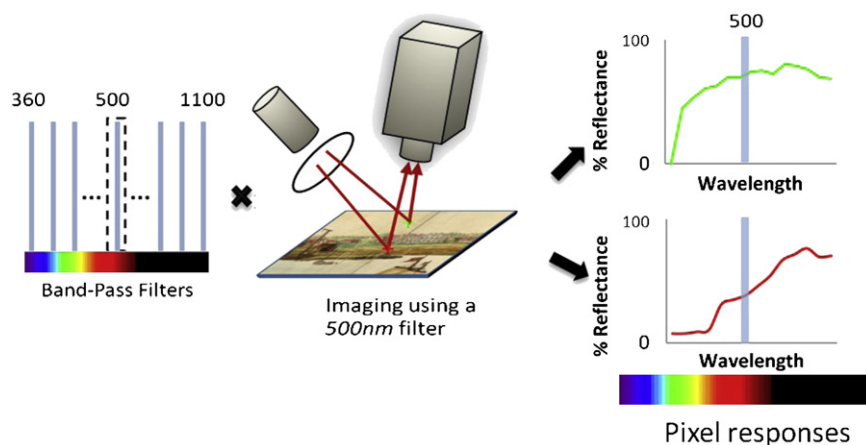


**Fig. 2.** Hyperspectral imaging process. At each scan, a monochrome camera measures the reflected light from the document surface. The document reflects a very narrow band of EM radiation due to the bandpass filter positioned in front of the light source (500 nm in this example). This process is repeated using 70 different bandpass filters to build the HSI.

closely as possible, while [20,21] attempt to recover underwritten text irrespective to original document's appearance.

## 2.2. Image fusion

Image fusion is another closely related topic to our work. There are several different categories in image fusion. Image fusion plays a vital role in remote sensing where the goal is to fuse different types of images from satellites or aircrafts to provide an increased visual saliency of the area being imaged. The types of imagery provided cover different portions of the electro-magnetic spectrum at different spatial, temporal, and spectral resolution [22]. In many cases, the focus of fusion techniques in remote sensing is to assist with the interpretation of the data in many cases by simple false-coloring. A comprehensive review of image fusion in remote sensing is offered in [23].

In computer vision and graphics, image fusion of flash/no-flash photographs has gained interest to assist in imaging in dark environments. In [24,25], flash images were used to significantly enhance details and reduce noise in ambient images. Both of these approaches use joint-bilateral filters to decompose images into detail and base layers, and reconstruct the image by combining the large scale of ambient image and the detail of the flash image. In [26], a gradient projection scheme for flash/no-flash image fusion was introduced with the goal more focused on the removal of flash artifacts. In related work, image fusion technique for combining images captured under different illumination for context enhancement was introduced in [27].

The closest work to ours is the multispectral image fusion methods introduced in [28–30]. In [28], a video taken in a low light environment is enhanced by fusing the visible-spectrum video with the video simultaneously captured with an infrared sensor. This work introduced a modified bilateral filter suited for multispectral imagery to essentially decompose the images to low frequency contents and details. In [29], low contrast photographs were enhanced with NIR images by incorporating texture information from NIR. They apply wavelet decomposition to decompose the image into low frequency and high frequency details similar to other methods. The details of the NIR image are transferred by histogram matching. An extension of flash/no-flash techniques to multispectral imaging was introduced in [30]. In their work, a prototype of camera and flash that also uses infrared and ultra-violet was presented. They exploit the correlations between images at different spectral bands to reduce noise and add fine details in the ambient image.

Our work can be viewed as the extension of the multispectral image fusion to hyperspectral image fusion.<sup>1</sup> In multispectral image fusion methods [28–30], images consist of three visible-spectrum images (RGB) and one extra image that integrates information in NIR (an extra UV image is included in [30]). In contrast, we deal with much more images densely sampled over a broad range of spectrums. The hyperspectral image examples shown in this paper contain 70 images sampled from 365 to 1100 nm. This brings more challenges to the fusion problem since there is significantly more information available. Hence, one of the main contributions of this paper is to present methods to detect regions in the visible-spectrum images that can be enhanced by using the information from NIR images and to extract a single map containing information to be fused from all the NIR images.

## 3. HSI document enhancement algorithm

As mentioned earlier, there are two types of enhancement that are targeted in this paper. With text documents, our algorithm aims to remove the undesired artifacts, notably ink-bleed, ink-corrosion, and foxing (age related spots). The final results are enhanced documents that still maintain the look of the original with the undesired artifacts significantly reduced. For this task, the images in the invisible range provide the source for the background of the enhanced image since invisible range images are much less affected by the corrosive artifacts. With documents that contain line drawings with low contrast that is attributed to ink-corrosion, our algorithm increases the contrast and adds image details not present in the visible range. For this task, the invisible range images are sources of foreground ink with salient gradient details.

While the data can be enhanced by modifying each spectral band image in the visible spectrum and then constructing an RGB image, we chose to enhance the RGB image of the hyperspectral data to reduce computation.<sup>2</sup> The enhancement is performed in

<sup>1</sup> The distinction between multispectral vs. hyperspectral is typically related to the number of bands as well as the manner in which the data is collected. We refer to our data as hyperspectral as it provides a densely sampled (10 nm intervals) spectral response from a single sensor.

<sup>2</sup> Note that there is no RGB image in the HSI data. The RGB image must be computed by applying synthetic lighting and integrating the visible spectral response.

the gradient domain and both tasks follow similar procedures. In the first step, pixels are segmented into two groups: a group that should remain the same (group A) and a group that needs to be enhanced (group B). A new gradient map is then composited by combining gradients from different spectral band images. For the pixels in the group A, the gradients remain unchanged. For the pixels in the group B, the gradients are replaced by the gradients from the invisible band images that suit the purpose of the task. Finally, output images are reconstructed from the gradient maps by an optimization scheme.

The following notations will be used throughout the paper. The term  $I_\lambda$  indicates the image of the data at a spectrum  $\lambda$ ,  $\mathbf{x}$  indicates a pixel location, and  $\mathbf{s}_x$  is the spectral response of the point  $\mathbf{x}$ :

$$\mathbf{s}_x = [I_{\lambda_1}(\mathbf{x}), I_{\lambda_2}(\mathbf{x}), \dots, I_{\lambda_m}(\mathbf{x})]^T.$$

In the following, we describe our algorithm starting with details for compositing gradient maps to reconstructing images from gradients.

### 3.1. Gradient map composite for artifact removal in text-based documents

Fig. 3 summarizes the algorithm for compositing a gradient map for the artifact removal tasks in text documents. The first step is to segment the input into foreground (texts) and background. In our system, we employ a simple user-assisted strategy where the user needs to only provide a mark-up on a small area that belongs to the foreground. After the segmentation, the mean spectrum of the foreground pixels ( $\bar{\mathbf{p}}$ ) is computed, then a similarity map  $S$  for all the pixels is computed (Fig. 3(b)):

$$S(\mathbf{x}) = 1 - \frac{\|\bar{\mathbf{p}} - \mathbf{s}_x\|^2}{m}, \quad (1)$$

where  $m$  is the number of spectral samples. After applying thresholding, we get a binary mask  $M$  which has 1's only in the foreground region. To composite a new gradient map ( $G$ ) for the enhancement, we use the gradient of the original image ( $\nabla I_i$ ) for the foreground and the gradient of an image from the invisible range ( $\nabla I_\lambda$ ,  $700 < \lambda < = 1100$ ) for the background. The band with the smallest variation in the background region is chosen for the  $I_\lambda$ . Hence, the gradient map  $G$  is generated as follows:

$$G = M \circ \nabla I_i + (1 - M) \circ \nabla I_\lambda. \quad (2)$$

The operator  $\circ$  is the Hadamard product. This procedure is applied individually to each of the RGB channel of the input image.

### 3.2. Gradient map composite for contrast enhancement in drawing-based documents

For the contrast enhancement task, the procedure is similar to the procedure for the artifact removal, but can be performed automatically. The first step is to determine which regions can be enhanced by using the additional information from the NIR bands. To do this, we use the observation that the local contrast of regions that can be enhanced with additional spectral bands is much higher in the NIR bands than the local contrast in the visible bands. In Fig. 4(a), the local contrast inside the drawings of the ships is extremely low in the visible bands (for example, points  $p1$  and  $p2$ ). The local contrast inside these regions greatly increases in the NIR bands as can be seen in Fig. 4(b) and (c). In contrast, the local contrasts remain constant throughout the spectrum in some other regions in the data (points  $p3$  and  $p4$ ). It is unnecessary to enhance these regions with additional bands and risk amplifying sensor noise. Using the insight explained above, we compute a saliency map ( $S$ , Fig. 5(a)) as follows:

$$S(\mathbf{x}) = \frac{1}{m'} \sum_{\lambda \in \text{NIR}} \max_{\mathbf{y} \in N(\mathbf{x})} |I_\lambda(\mathbf{x}) - I_\lambda(\mathbf{y})| - \max_{\mathbf{y} \in N(\mathbf{x})} |I_i(\mathbf{x}) - I_i(\mathbf{y})|, \quad (3)$$

where  $I_i$  is the input image,  $N(\mathbf{x})$  refers to the neighbors of  $\mathbf{x}$ , and  $m'$  is the number of spectral bands in the NIR. In this paper, we use the size of  $7 \times 7$  for the neighborhood.

After thresholding the saliency map  $S$  with a morphological operation to increase its size slightly, we again obtain a binary mask  $M$  as the previous task (Fig. 5(b)). The foreground mask  $M$  has 1's only in the region where the enhancement is necessary. A new gradient map  $G$  for the enhancement is computed as follows:

$$G = M \circ G' + (1 - M) \circ \nabla I_i. \quad (4)$$

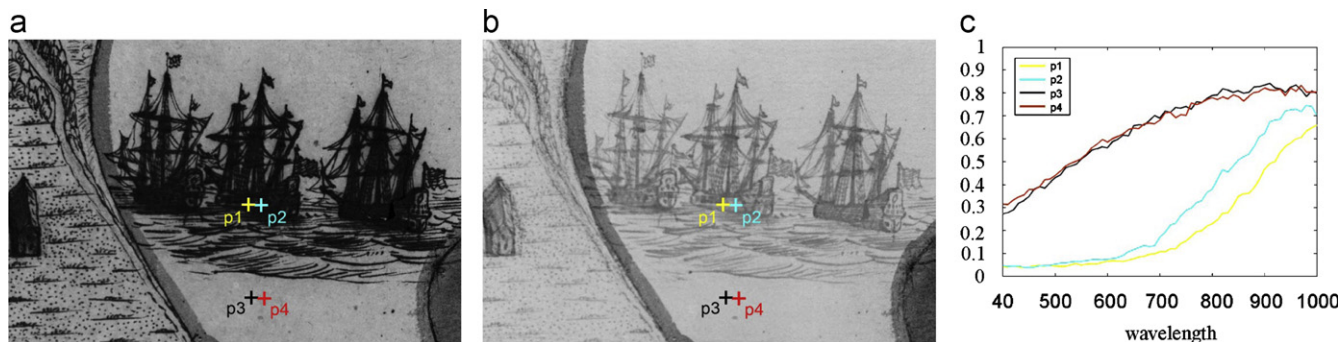
Determining the new gradient  $G'$  in Eq. (4) is the key to enhancing the details in the original image. One option for computing  $G'$  is to select a band in NIR with high contrast similar to choosing a band with lowest variation as the background in Section 3.1. This may not be the best choice since we have observed that different regions in the image have higher contrast in different NIR bands. Hence one suitable option for computing  $G'$  is to integrate information from all available NIR bands and choose different bands to provide the strongest gradients for each pixel in these regions. To maintain spatial consistency in this gradient assignment we formulate the problem as a Markov Random Field (MRF) where each pixel  $\mathbf{x}$  is assigned a label  $l_x \in \text{NIR}$ . To solve the MRF, the following energy is minimized in order to find optimal pixel labels:

$$E = E_d + \omega E_s, \quad (5)$$

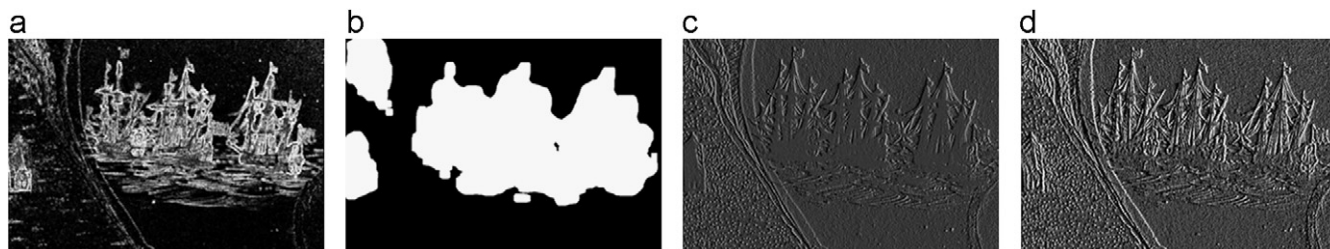
where  $E_d$  is the data-cost energy reflecting the likelihood of assigning a label to each pixel,  $E_s$  is the smoothness energy



Fig. 3. Gradient map construction for text documents: (a) input image and an user mark-up, (b) similarity map  $S$ , (c) gradients for foreground  $\nabla I_i$  and background  $\nabla I_\lambda$ , (d) gradient composite  $G$ .



**Fig. 4.** We detect regions where the local contrast is much higher in the NIR bands than the visible bands to apply enhancement using the NIR bands. (a) image at 500 nm. (b) image at 900 nm. (c) spectral plots.



**Fig. 5.** Gradient map composition for enhancement: (a) saliency map  $S$  (Eq. (3)), (b) binary mask  $M$ , (c) original gradient map  $\nabla I_i$ , (d) new gradient composite  $G$ .

representing the cost of assigning different labels to adjacent pixels, and  $\omega$  is the weight that controls the strength of the smoothness term. The data cost  $E_d$  is computed as follows:

$$E_d(l_{\mathbf{x}} = \lambda) = -|\nabla I_{\lambda}(\mathbf{x})|, \quad \lambda \in \text{NIR}. \quad (6)$$

We enforce smoothness on adjacent pixels  $(\mathbf{p}, \mathbf{q})$  with the following smoothness cost:

$$E_s(l_{\mathbf{p}}, l_{\mathbf{q}}) = |l_{\mathbf{p}} - l_{\mathbf{q}}|. \quad (7)$$

Our MRF is optimized using the Middlebury MRF library [31] with the graph-cuts solver [32]. After the labeling is complete, the gradient map  $G$  is constructed as follows:

$$G(\mathbf{x}) = \nabla I_{\mathbf{x}}(\mathbf{x}). \quad (8)$$

### 3.3. Image reconstruction from a gradient map

We now have to reconstruct an image from the gradient map computed in Eqs. (2) or (4). The goal is to reconstruct an image  $R$  in which the intensities are close to the input image  $I_i$  and the gradients are close to the computed gradient map  $G$ . We use the following cost function for the reconstruction which is similar to the one used in [30]

$$\operatorname{argmin}_R \sum_{\mathbf{x}} [\gamma |R(\mathbf{x}) - I_i(\mathbf{x})|^2 + |\nabla_x R(\mathbf{x}) - \beta G_x(\mathbf{x})|^\alpha + |\nabla_y R(\mathbf{x}) - \beta G_y(\mathbf{x})|^\alpha], \quad (9)$$

The first term in Eq. (9) forces  $R$  to be close to the input image  $I_i$  under an  $\ell^2$  norm. The second and the third term make the gradients of the reconstructed image  $R$  to be close to the gradient map  $G$  under a sparse norm ( $\alpha \leq 1$ ) where sub-indices  $x, y$  refer to the gradient directions. Using the sparse norm on the gradient terms encourages the edge structures in  $R$  to align spatially with those in  $G$  in contrast to the  $\ell^2$  norm where  $\nabla R$  will be matched closely with  $G$  [30]. The parameter  $\gamma$  controls the balance between the effect of the first term and the gradient terms. The parameter  $\beta$  controls the strength of the gradient composite on the final image.

To optimize Eq. (9), we modified the fast optimization scheme used for image deconvolution recently introduced in [33]. With this optimization scheme, we were able to process our reconstruction in 20 s per channel, a significant improvement over the suggested solver in [34,30] which required 8 min per channel.

## 4. Experiments

The first set of experiments target the removal of artifacts on the documents. The document in the first example (Fig. 6) is visually corrupted with foxing. The result of our enhancement algorithm is shown in Fig. 6(b). The foxing artifact is greatly reduced in the enhanced image while the texture and the look of the original image is preserved. The ability to preserve the look and feel is one significant advantage offered by having the additional gradients in the NIR information. In related document processing work [13–15,19], the output of the artifact removal is a binary image with a uniform color background and a color for the foreground. While the binarization enhances the ability to interpret the data, the texture and the look of the original document is completely lost. This is shown in Fig. 6(c) where the background is filled with the mean RGB of the background in the original image with a Gaussian noise (to simulate the paper texture). As can be seen, this looks unnatural compared with the HSI enhancement. Another example of artifact removal is shown in Fig. 7. In this example, a document is corrupted with mild ink-bleed. Using our method, the ink-bleed artifact is removed while the textures and the lines in the original image are preserved. Note that the watermark in the original image is also preserved in our reconstruction. While thresholding could be used to remove the ink-bleed for this input, replacing the background with the mean RGB completely loses the feel and important features such as lines and the watermark of the document (Fig. 7(c)). The document in Fig. 8(a) is significantly more affected by ink-bleed and corrosion. The artifacts are greatly reduced using algorithm as can be seen in Fig. 8(b). Some artifacts can be still seen in this example because the spectrum of the pixels with strong ink-bleeds have the same spectral properties as the foreground text. Additional

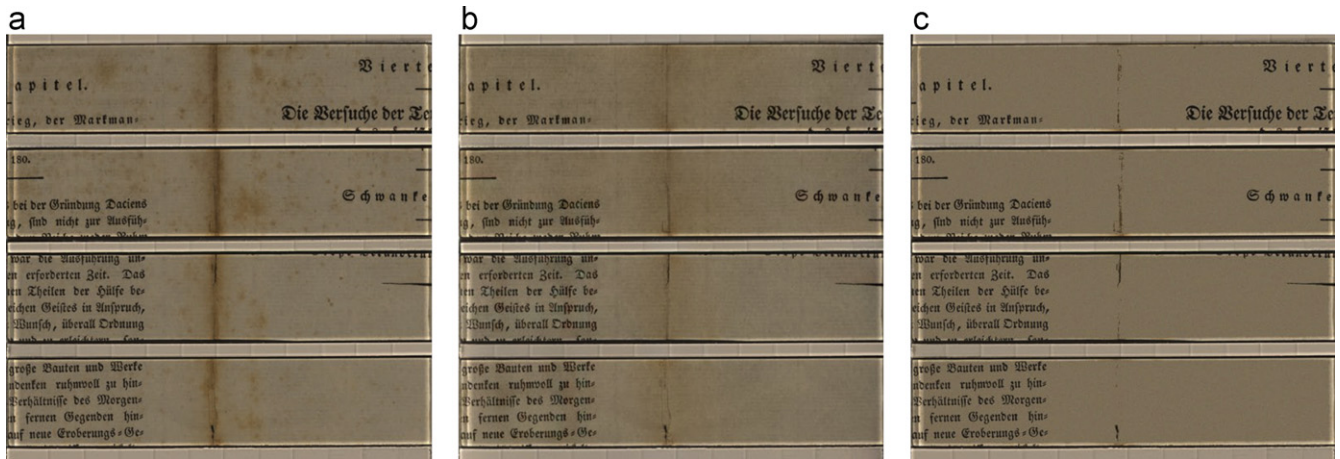


Fig. 6. (a) The original RGB image is visually enhanced by reducing the foxing artifact. (b) With the hyperspectral data, the enhanced image preserves the texture and the look of the original image. (c) Image reconstructed by replacing the background with the mean value does not look natural.

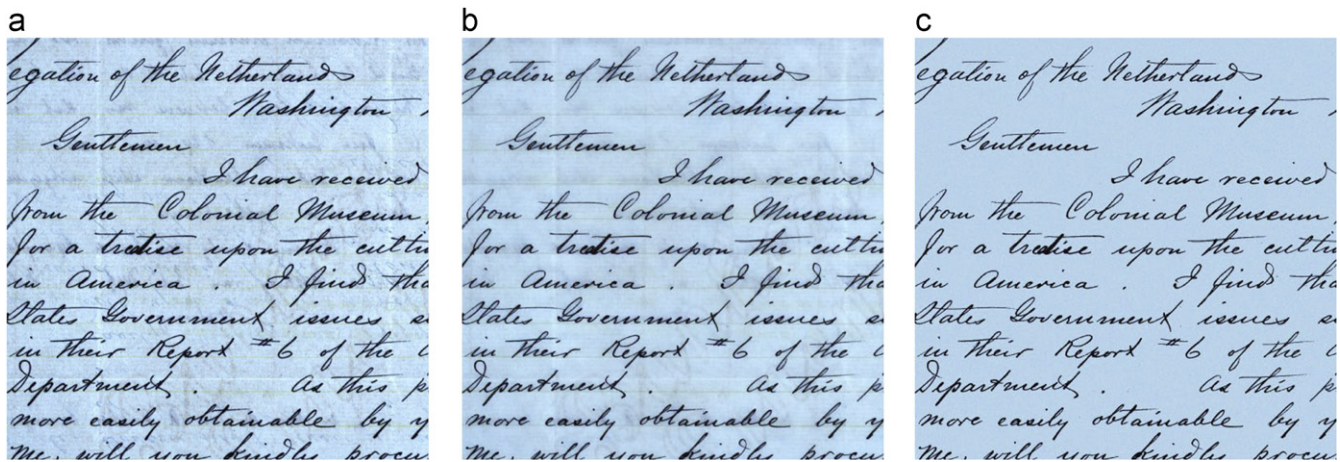


Fig. 7. (a) The original RGB image is visually enhanced by removing the ink-bleed artifact. (b) With the hyperspectral data, the enhanced image preserves the texture and the look of the original image. Note that the watermark and the underlines on the image are preserved. (c) Image reconstructed by replacing the background with the mean value completely loses the look of the original document.

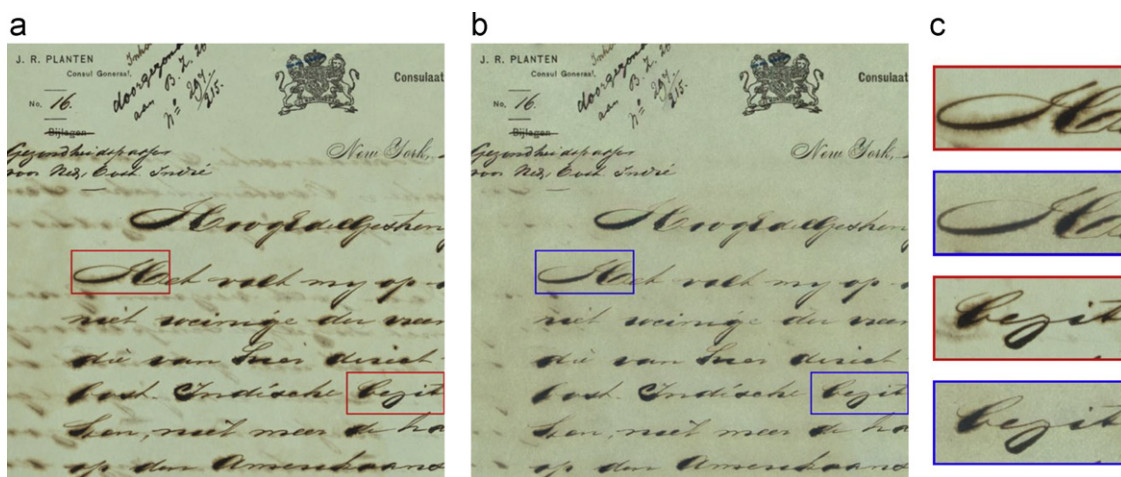
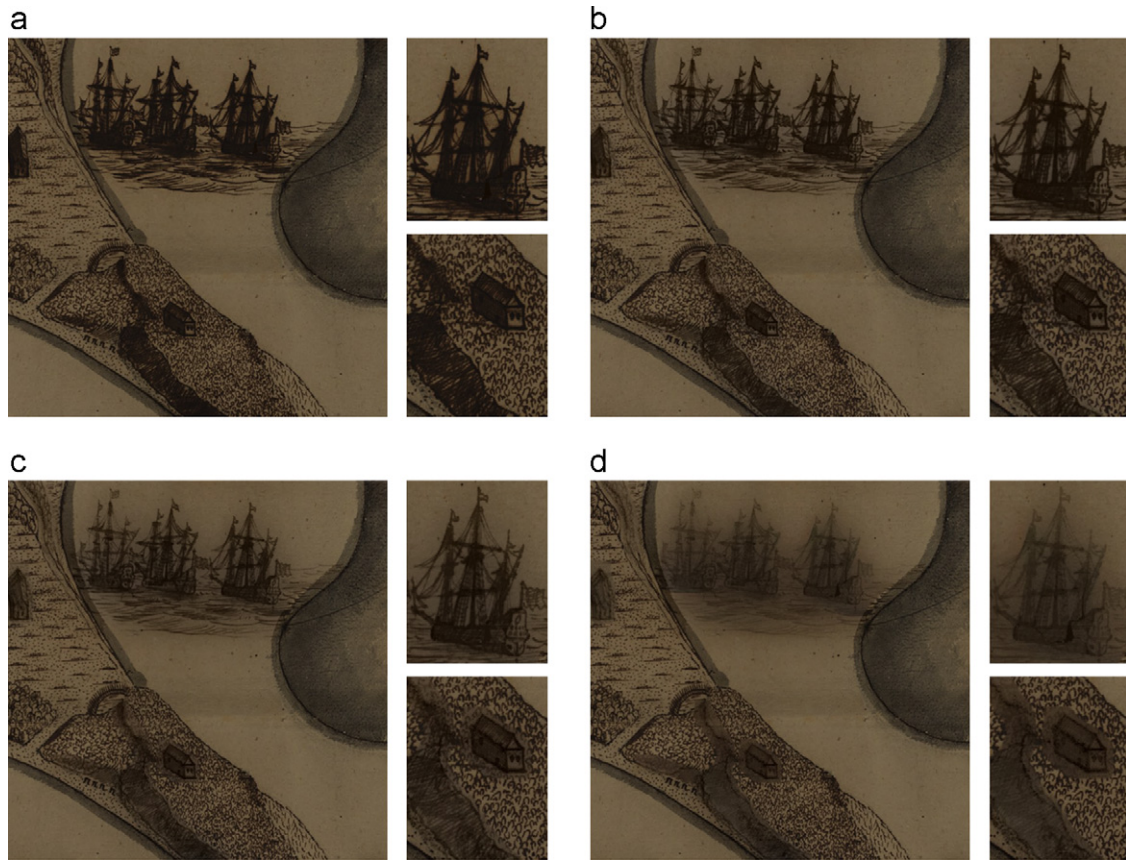


Fig. 8. (a) The original document contains severe ink-bleed and corrosion artifacts. (b) The artifacts are reduced and the image is visually enhanced with our algorithm. A close views of selected regions are shown in (c).

user assistance such as in [19] could be used for further enhancement of the document in this case.

Next, we show results on the contrast enhancement of documents with line drawings. Fig. 9(a) shows a part of early map of

Syracuse drawn circa 1700. Due to corrosion, contrast in some parts of the map decreased resulting in the loss of details (see close-up view in Fig. 9(a)). We first test contrast enhancement by using just one NIR band as the source for the gradient map as the



**Fig. 9.** Original image with low contrast in some parts (RGB, (a)) is enhanced using images in NIR range. Using just one NIR band does not give satisfactory results since one band does not capture the best contrast for all regions. Hence a scheme for integrating information from all NIR bands is necessary. (a) Original image in RGB. (b) Image enhanced with 750 nm. (c) Image enhanced with 850 nm. (d) Image enhanced with 950 nm.

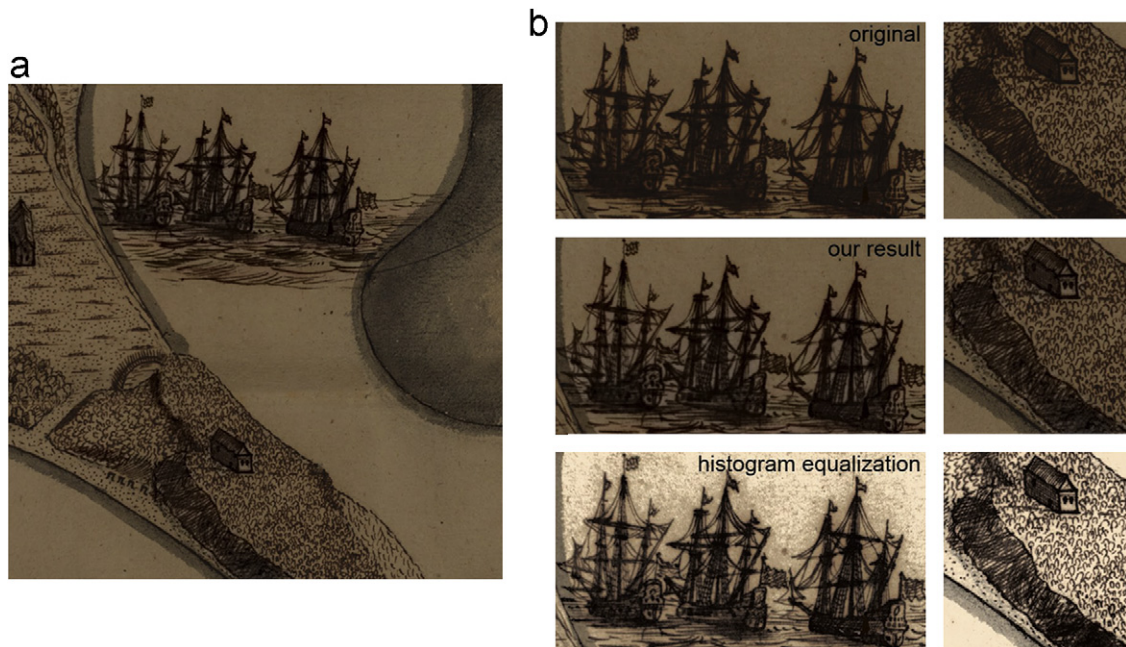


**Fig. 10.** (a) The enhancement result using our algorithm. The contrast is greatly enhanced and the details on the ships and on the houses is now recovered. (b) Close-up views of the original RGB image (top), our enhancement result (middle), and histogram equalization result (bottom).

artifact removal examples. Fig. 9(b)–(d) show enhancement results using NIR images at 750, 850, and 950 nm respectively. Since images at different wavelength show different contrast in

different regions, one image is not enough to yield enhancement in all areas. For example, while the house region is enhanced well in Fig. 9(b), the details of the textures on the ships are still not

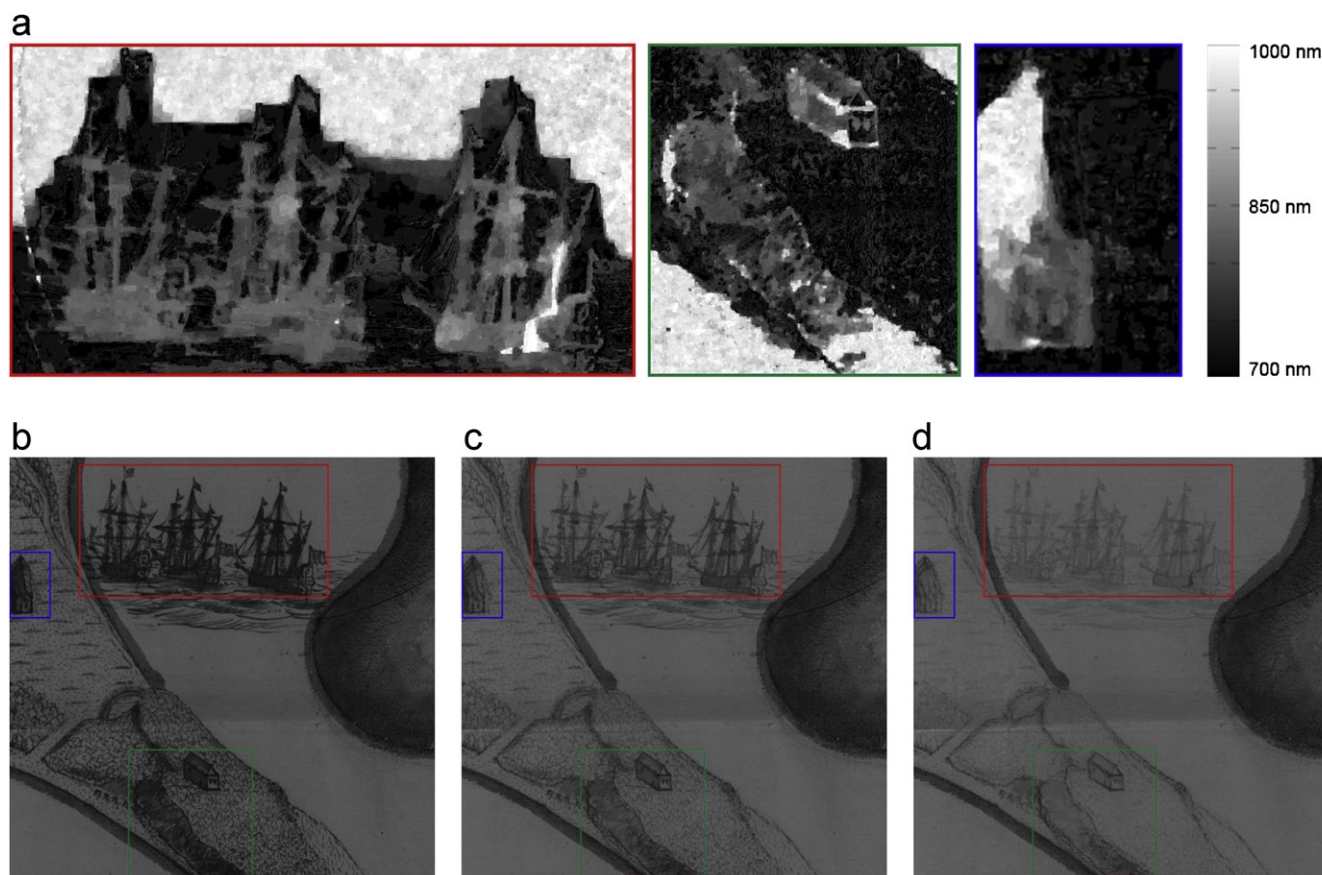


**Fig. 11.** Labels for the gradient map composite: (a) labeling of pixels indicates which band image (nm) to use to get gradients, (b) image at 720 nm, (c) image at 880 nm, (d) image at 1000 nm.

apparent in this image. While the details of the ships are recovered with the image at 850 nm (Fig. 9(c)), the area with the house is blurred due to low gradients in this region at this wavelength. Both areas are washed out at 950 nm, but this image provides the most clear view of the hole in one of the ships (see the closed-up view in Fig. 9(d)). Hence, the best strategy for enhancing contrast in documents with line drawings would be to integrate information from all available NIR bands as we proposed in Section 3.2. Fig. 10 shows the result of our contrast enhancement. Details lost in the original RGB image are recovered and all regions are equally enhanced in contrast to the results from using just one band (Fig. 9). Fig. 11 shows some of the labeling results by our MRF framework. As can be seen from the labeling map, information from different bands are integrated. For example, lower NIR band images were used to provide strong boundaries of the ships, mid NIR band images were used to provide details inside the ships, and the highest NIR band image was used to distinguish the hole in one of the ships. Our enhancement result is compared with the enhancement using local histogram equalization in Fig. 10. While the contrast is enhanced and the details are revealed by applying histogram equalization locally to each region, the noise is also amplified and the original color is lost in the process. We also applied global histogram equalization to the whole image which did not give a satisfactory result.

## 5. Discussion

We have described how to take advantage of hyperspectral imaging, most notably using images in near-infrared to assist in

visually enhancing old documents. Specifically, we demonstrated how to improve the visual quality of text-based documents corrupted with artifacts such as ink-bleed, ink-corrosion, and foxing, by using the invisible bands to help remove these undesired artifacts. For documents with line drawings that suffer from low contrast, we use the invisible bands to provide more details to enhance legibility. The key components of our framework included detecting regions that can be enhanced by NIR range images, compositing the enhanced gradient map from NIR images, and reconstructing the final image from gradients using an optimization scheme.

The feedback from our collaborators at the NAN has been highly positive. Our algorithms have been integrated as part of a comprehensive HSI visualization tool used by the NAN. In particular, they state that this algorithm can be used to produce results that augment physical exhibitions, where a printout of the enhanced version produced by our algorithm is displayed near the original document. The ability to maintain the look and feel of the original document was especially lauded, as previous attempts by themselves was done with less success in Photoshop.

As future work, we plan to work on segmenting the document artifacts from the foreground ink that are less sensitive to thresholding. In some cases such as in Fig. 8, spectrums of strong ink-bleeds and corruptions are very similar to the foreground spectrum which make the segmentation results rely greatly on the thresholding. Since choosing an optimal threshold is often challenging, some of the foreground texts may be removed while removing the document artifacts as can be seen in Fig. 8(c). We can employ a more sophisticated user assistance as in [19] for further enhancement of the document. Additionally, we plan to consider extracting several spectral bands that are more powerful in distinguishing the

foreground rather than using the entire HSI spectrums. This allows to use only a few bands for similarity analysis, as prior research in the archival domain has established that certain bands are more suitable for various tasks and materials being observed. This selective band strategy can also be used to amplify desired artifacts, such as tears and rips, and for managing future data collection in which only the useful bands may need to be captured.

## Acknowledgments

We gratefully acknowledge the support and efforts from our collaborators Roberto Padoan from the Nationaal Archief of the Netherlands (NAN) and Marvin Klein from Art Innovation. This work was supported in part by the NUS Young Investigator Award, R-252-000-379-101.

## References

- [1] H. Li, C.-W. Fu, A. J. Hanson, Visualizing multiwavelength astrophysical data, in: *IEEE Transactions on Visualization and Computer Graphics* (Proceedings of IEEE Visualization), vol. 14, 2008, pp. 1555–1562.
- [2] C. Collet, M. Louys, A. Oberto, C. Bot, Markov model for multispectral image analysis: application to small magellanic cloud segmentation, in: *Proceedings of IEEE International Conference on Image Processing*, 2003, pp. 953–956.
- [3] M.A. Loghmari, M.S. Naceur, M.R. Boussema, A spectral and spatial source separation of multispectral images, *IEEE Transactions on Geoscience and Remote Sensing* 44 (2006) 3659–3673.
- [4] Q. Du, C.-I. Chang, A linear constrained distance-based discriminant analysis for hyperspectral image classification, *Pattern Recognition* 34 (2001) 361–373.
- [5] Z. Pan, G. Healey, M. Prasad, B. Tromber, Face recognition in hyperspectral images, *IEEE Transactions on Pattern Analysis and Machine Intelligence* 25 (2003) 1552–1560.
- [6] R. Padoan, T. Steemers, M. Klein, B. Aalderink, G. de Bruin, Quantitative hyperspectral imaging of historical documents: technique and applications, in: *International Conference on NDT of Art*, 2008.
- [7] P. Cotte, D. Dupraz, Spectral imaging of leonardo da vinci mona lisa: an authentic smile at 1523 dpi with additional infrared data, in: *Proceedings of IS&T Archiving Conference*, 2006, pp. 228–235.
- [8] P. Pérez, M. Gangnet, A. Blake, Poisson image editing, in: *ACM Transactions on Graphics* (Proceedings of SIGGRAPH), vol. 22, 2003, pp. 313–318.
- [9] R. Fattal, D. Lischinski, M. Werman, Gradient domain high dynamic range compression, in: *ACM Transactions on Graphics* (Proceedings of SIGGRAPH), 2002.
- [10] A. Levin, A. Zomet, S. Peleg, Y. Weiss, Seamless image stitching in the gradient domain, in: *Proceedings of European Conference on Computer Vision*, 2004.
- [11] Y. Weiss, Deriving intrinsic images from image sequences, in: *Proceedings of IEEE International Conference on Computer Vision*, 2001, pp. 68–75.
- [12] M. Klein, B.J. Aalderink, R. Padoan, G. de Bruin, T.A.G. Steemers, Quantitative hyperspectral reflectance imaging, *Sensors* 8 (2008) 5576–5618.
- [13] Z. Shi, V. Govindaraju, Historical document image enhancement using background light intensity normalization, in: *Proceedings of IEEE International Conference on Pattern Recognition*, 2004.
- [14] C.L. Tan, R. Cao, P. Shen, Restoration of archival documents using a wavelet technique, *IEEE Transactions on Pattern Analysis and Machine Intelligence* 24 (2002) 1399–1404.
- [15] Y. Huang, M.S. Brown, D. Xu, A framework for reducing ink-bleed in old documents, in: *Proceedings of IEEE Conference on Computer Vision and Pattern Recognition*, 2008, pp. 1–8.
- [16] L. Zhang, A.M. Yip, M.S. Brown, C.L. Tan, A unified framework for document restoration using inpainting and shape-from-shading, *Pattern Recognition* 42 (2009) 2961–2978.
- [17] C. Wolf, Document ink bleed-through removal with two hidden Markov random fields and a single observation field, *IEEE Transactions on Pattern Analysis and Machine Intelligence* 32 (2010) 431–447.
- [18] R.F. Moghaddam, M. Cheriet, Low quality document image modeling and enhancement, *International Journal on Document Analysis and Recognition* 11 (2009) 183–201.
- [19] Z. Lu, Z. Wu, M. Brown, Directed assistance for ink-bleed reduction in old documents, in: *Proceedings of IEEE Conference on Computer Vision and Pattern Recognition*, 2009.
- [20] K. Knox, Enhancement of overwritten text in the archimedes palimpsest, *Computer Image Analysis in the Study of Art*, Proceedings of SPIE 6810 (2007).
- [21] E. Salerno, A. Tonazzini, L. Bedini, Digital image analysis to enhance underwritten text in the archimedes palimpsest, *International Journal on Document Analysis and Recognition* 9 (2007) 79–87.
- [22] C.H. Chen, P.P. Ho, Statistical pattern recognition in remote sensing, *Pattern Recognition* 41 (2008) 2731–2741.
- [23] C. Pohl, J.L.V. Genderen, Multisensor image fusion in remote sensing: concepts methods and applications, *International Journal of Remote Sensing* 19 (1998) 823–854.
- [24] E. Eismann, F. Durand, Flash photography enhancement via intrinsic relighting, in: *ACM Transactions on Graphics* (Proceedings of SIGGRAPH), vol. 23, 2004, pp. 673–678.
- [25] G. Petschnigg, R. Szeliski, M. Agrawala, M.C.H. Hoppe, K. Toyama, Digital photography with flash and no-flash image pairs, in: *ACM Transactions on Graphics* (Proceedings of SIGGRAPH), vol. 23, 2004, pp. 664–672.
- [26] A. Agrawala, R. Raskar, S.K. Nayar, Y. Li, Removing photography artifacts using gradient projection and flash-exposure sampling, in: *ACM Transactions on Graphics* (Proceedings of SIGGRAPH), vol. 24, 2005, pp. 828–835.
- [27] R. Raskar, A. Ilie, J. Yu, Image fusion for context enhancement and video surrealism, in: *International Symposium on Non-Photorealistic Animation and Rendering*, 2004, pp. 85–93.
- [28] E. Bennett, J.L. Mason, L. McMillan, Multispectral bilateral video fusion, *IEEE Transactions on Image Processing* 16 (2007) 1185–1194.
- [29] X. Zhang, T. Sim, X. Miao, Enhancing photographs with near infrared images, in: *Proceedings of IEEE Conference on Computer Vision and Pattern Recognition*, 2008, pp. 1–8.
- [30] D. Krishnan, R. Fergus, Dark flash photography, in: *ACM Transactions on Graphics* (Proceedings of SIGGRAPH), 2009.
- [31] R. Szeliski, R. Zabih, D. Scharstein, O. Veksler, V. Kolmogorov, A comparative study of energy minimization methods for Markov random fields, in: *Proceedings of European Conference on Computer Vision*, 2006.
- [32] Y. Boykov, V. Kolmogorov, An experimental comparison of min-cut/max-flow algorithms for energy minimization in vision, *IEEE Transactions on Pattern Analysis and Machine Intelligence* 26 (2004) 1124–1137.
- [33] D. Krishnan, R. Fergus, Fast image deconvolution using hyper-Laplacian priors, in: *Proceedings of Neural Information Processing Systems*, 2009.
- [34] A. Levin, Y. Weiss, User assisted separation of reflections from a single image using a sparsity prior, *IEEE Transactions on Pattern Analysis and Machine Intelligence* 29 (2007) 1647–1654.

**Seon Joo Kim** received B.S. and M.S. degrees from Yonsei University, Seoul, Korea, in 1997 and 2001. He received Ph.D. degree in computer science from University of North Carolina at Chapel Hill in 2008. He is currently a research fellow in National University of Singapore. He has worked as an intern at Cortex and GE Global Research Center during the summers of 2004 and 2005, respectively. His research interests include computer vision, image/video analysis, and computational photography where he has published in major computer vision conferences and journals. He received the Ministry of Information and Communication Scholarship (Republic of Korea) in 2002 and the Graduate School Dean Scholarship (Yonsei University) in 1999.

**Fanbo Deng** received his B.S. in Computer Science from the Harbin Institute of Technology, China, in 2008. He is currently a Ph.D. student at the National University of Singapore. His research focus is on Computer Vision, Image Processing, and Visualization.

**Michael S. Brown** obtained his B.S. and Ph.D. in Computer Science from the University of Kentucky in 1995 and 2001, respectively. He was a visiting Ph.D. student at the University of North Carolina at Chapel Hill from 1998–2000. He is currently an Associate Professor in the School of Computing at the National University of Singapore. Dr. Brown regularly serves on the program committees for the major Computer Vision conferences (ICCV, CVPR, and ECCV) and as an Area Chair for CVPR. He served as the general co-chair for the 5th Projector-Camera-Systems (PROCAMS'08) workshop co-located with SIGGRAPH'08 and was an organizer for the 1st eHeritage'09 workshop co-located with ICCV'09. His research interests include Computer Vision, Image Processing and Computer Graphics.